COBEM 2023 27TH INTERNATIONAL CONGRESS OF MECHANICAL ENGINEERING

ABCM Brazilian Society of Mechanical Sciences and Engineering
27th ABCM International Congress of Mechanical Engineering
December 04-08, 2023, Florianópolis-SC, Brazil

COB-2023-1188

DYNAMIC BEHAVIOR ANALYSIS OF A FRAME WITH ROTATIONAL FRICTION DAMPER BY NUMERICAL AND EXPERIMENTAL METHOD

Fabrício do Amaral Cristóvão
Antonio Almeida Silva
Academic Unit of Mechanical Engineering, Federal University of Campina Grande -UFCG
Av. Aprígio Veloso, 58428-830, Campina Grande- PB, Brazil
fabricio.amaral@estudante.ufcg.edu.edu.br
antonio.almeida@professor.ufcg.edu.br

Andersson Guimarães Oliveira
Mechanical Engineering Department, Federal University of Paraíba - UFPB
anderssonoliveira@gmail.com

José Sávyo Soares Lira
Academic Unit of Mechanical Engineering, Federal University of Campina Grande -UFCG
Av. Aprígio Veloso, 58428-830, Campina Grande- PB, Brazil
josesavyo.lira@ee.ufcg.edu.br

Handerson Patrick Moreira Valdevino
Academic Unit of Mechanical Engineering, Federal University of Campina Grande -UFCG
Av. Aprígio Veloso, 58428-830, Campina Grande- PB, Brazil
handerson.valdevino@gmail.com

Abstract. *The control of vibration amplitudes in structures is a highly relevant topic in the scientific-technological context, since the study of vibratory phenomena is essential to predict the dynamic behavior, extrapolating the effect of its dynamic response under external events, thus avoiding structural failures. In this paper shows a numerical-experimental procedure to analyze the dynamic behavior of a one-degree-of-freedom frame structure after the incorporation of a rotational friction damper. This damper is a device composed of aluminum disks that rotate in opposite directions, producing friction between their sliding surfaces. A compression coil spring works to apply the normal force to the friction surface, which also allows the determination of the normal force to the sliding plane from its deformed configuration, whose arrangement is mounted on a screw in the center of the damper. The behavior of the mechanism was characterized by base excitation tests under controlled conditions, exhibiting hysteresis of the same order of magnitude for a variation of cycles, which is linearly dependent on the displacement amplitude and normal force. Harmonic loads were applied, varying input parameters such as displacement amplitude, excitation frequency, and normal force. The results show that the use of the rotational friction damper as an additional damping system is capable of dissipating a large amount of vibrational energy and attenuating the vibration amplitudes of a structure, as well as providing a small increase in stiffness before the mechanism is activated, which could be an advantage over other conventional devices.*

Keywords: *rotational friction damper, experimental analysis, numerical analysis, dynamic behavior, hysteretic damping.*

1. INTRODUCTION

The growing demand to reduce and control the vibration amplitudes in structures motivates the of dynamic vibration absorbers (DVA) has proven to be an efficient and cost-effective strategy. This is particularly important in the face of devastating events such as earthquakes, seismic shocks, strong winds, among others.

(DVA) involve the incorporation of a secondary mass-spring system, coupled to the primary system, aiming to energy absorbing, particularly in the resonance region. This region corresponds to the natural frequency of the primary system, creating an anti-resonance region (Inman, 2013).

According to Kim et al. (2011), friction dampers are considered one of the most efficient energy-absorbing devices for building structures against earthquake loads. As soon as the structure undergoes lateral deformations, the friction dampers are activated and begin to dissipate energy, as illustrated in “Figure 1”. Since the dampers can dissipate a significant portion of the seismic energy, the forces acting on the structure can be considerably reduced. Coulomb

damping occurs when two dry surfaces slide relative to each other, depending on the velocity variation and the normal force between the sliding surfaces (Rao, 2010).

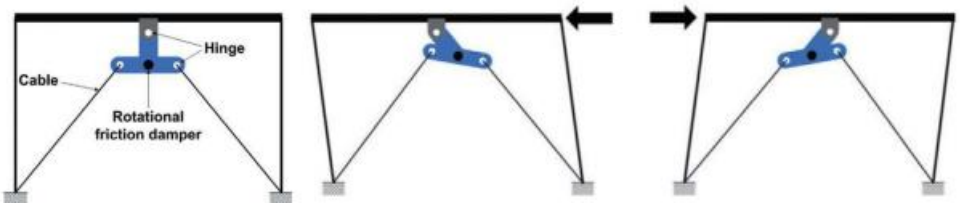

Figure 1. Mechanism of the rotational friction damper. (adapted from Kim et al. (2011))

2. THEORETICAL BACKGROUND

According to Inman (2013), Coulomb damping is a common damping phenomenon, often encountered in machines and structures, caused by sliding friction or dry friction. Coulomb damping is characterized by "Eq. (1)", where fc represents the dissipation force, N is the normal force, and μ is the coefficient of sliding friction.

$$f_c = F_c(\dot{x}) = \begin{cases} -\mu N & if\ \dot{x} > 0 \\ 0 & if\ \dot{x} = 0 \\ \mu N & if\ \dot{x} < 0 \end{cases} \tag{1}$$

Based on the model depicted in "Figure 2-a)", which free body diagram is presented in the "Figure 2-b)" and "Figure 2-c)", the friction force fc always opposes the direction of motion, making a system with Coulomb friction nonlinear.

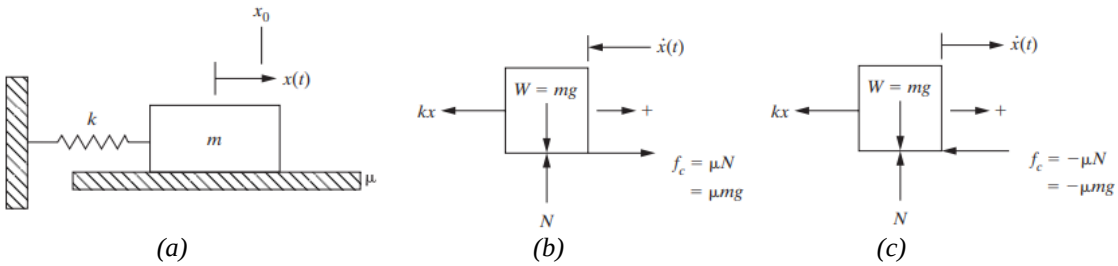

(a) *(b)* *(c)*

Figure 2. Spring-mass system with Coulomb damping. (adapted from Inman (2013))

Thus, equations of motion are written for the mass moving to the right and to the left, respectively. However, it is possible to unify them into a single equation using the approach presented in "Eq. (1)", as follows:

$$m\ddot{x} + \mu mgsgn(\dot{x}) + kx = 0 \tag{2}$$

Where *m* and *k* are the mass and stiffness, respectively; *sgn* is a signum function that plays the role of identifying the velocity $\dot{x}$ over time. Based on Inman (2013), this is a typical nonlinear system in which the concept of a single equilibrium position is lost. Thus, a continuous region of equilibrium positions exists. Since "Eq. (2)" is a nonlinear differential equation, a simple analytical solution does not exist, and numerical methods must be used to solve it (Rao, 2010).

3. METHODOLOGY

The frame prototype consists of a platform supported by two elastic columns. The rotational damper illustrated in "Figure 3" is composed of aluminum disks that rotate in opposite directions, generating friction between their sliding surfaces. A compression coil spring is used to apply the normal force to the friction surface, in order to induce the normal force on the sliding plane from its deformed configuration. The compressive force under surfaces is obtained by the coil spring deformation. This arrangement is mounted on a screw located at the center of the damper. To minimize undesirable friction between the rotating parts, a ball bearing is used in the support connection, in the vertical rod, aiming to maximize the efficiency of the damper.

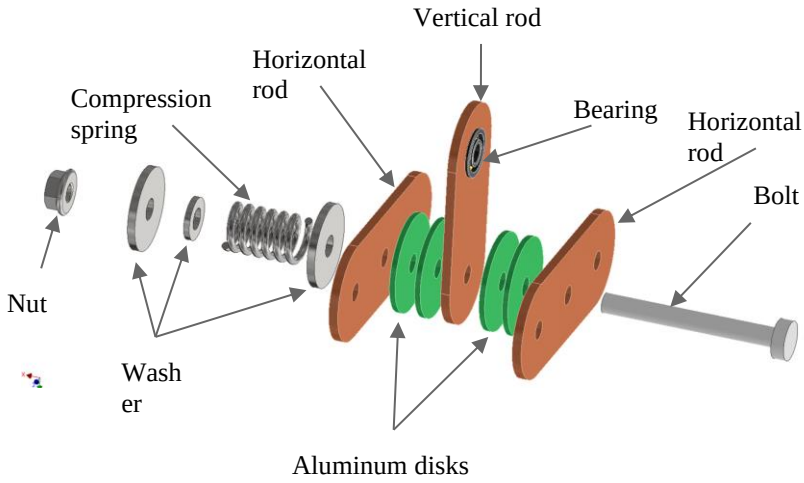

Figure 3 - Rotational friction damper proposed.

The device, as shown in "Figure 4", is connected to the structure through a V-shaped bracing system and linked to two pre-tensioned rods.

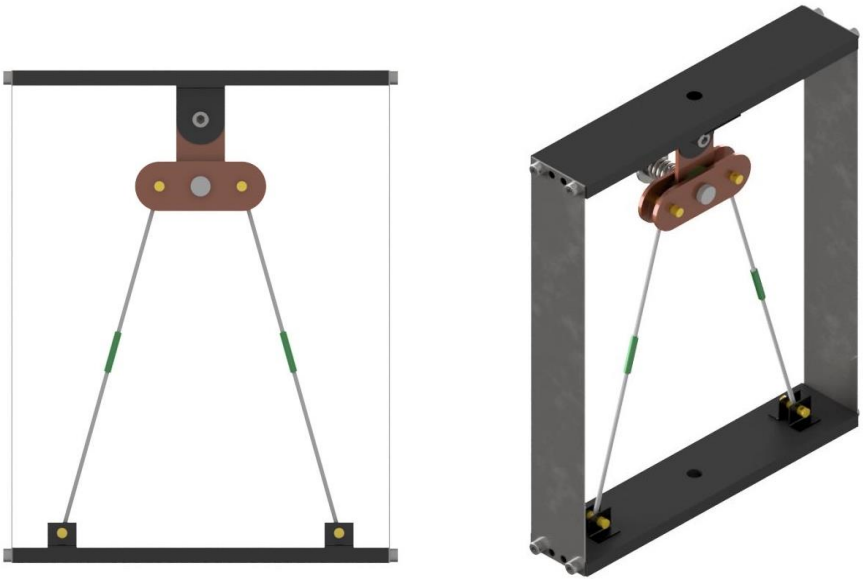

(a) *(b)*

Figure 4 – Prototype: (a) Front view; (b) Isometric view.

3.1 Characterization of the helical compression spring

The choice of the compression spring responsible for the application of forces on the contact surfaces by friction, it was necessary to determine the stiffness constant of the most suitable spring, through compression tests using the INSTRON, model 5582, as shown in “Figure 5”, with details of its fixation. Applying an initial preload of 2 N until reaching 44 N, and the data were treated in the Matlab® software.

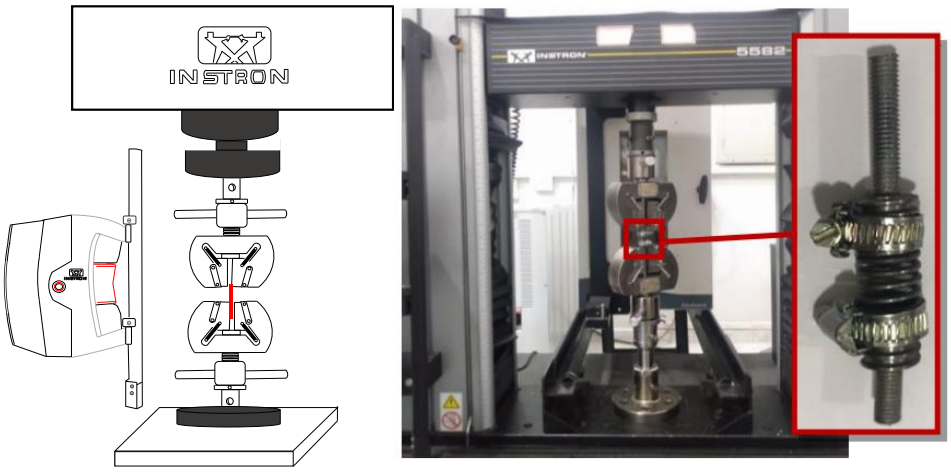

(a) *(b)*

Figure 5 – (a) INSTRON Setup template; (b) Experimental setup of the compression spring at INSTRON.

3.2. **Experimental and numerical modal analysis**

In the free vibration test, the frame was equipped with a PCB Piezotronics accelerometer model 352C68 with a sensitivity of 10 mV/g. For the excitation of the structure, a PCB Piezotronics impact hammer model 086D05-G was used, as shown in “Figure 6-(a)”. The input signals (hammer impact) and output signals (acceleration response) were collected using the Keysight Technologies dynamic signal analyzer model 35670A. “Figure 6-(b)” presents the finite element discretized mesh model of the frame.

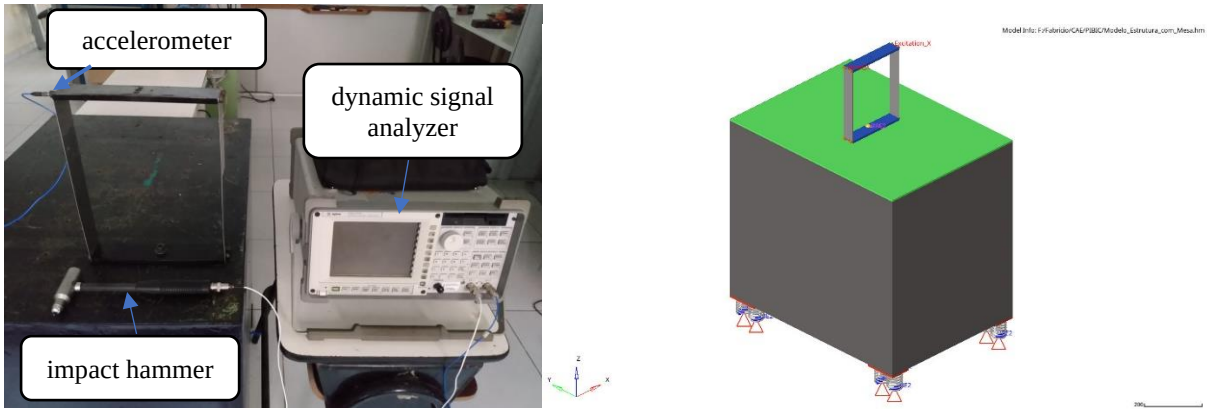

(a) *(b)*

Figure 6 - (a) Photograph of the experimental modal model of the frame; (b) Finite element model of the frame.

Utilizing the data from the previous phase, the finite element model was constructed in Altair® Hypermesh®, using a mixed mesh predominantly composed of tetrahedral elements, totaling 208,407 elements with a size of 5 mm. The "Inertial base" of the system was fixed, as shown in “Figure 6-(b)”. Friction between structural components and contact between metal joints were neglected to simplify the model.

3.3. **Characterization of the rotational friction damper**

To quantify the dissipated energy by the friction damper, forced excitation tests were conducted using an experimental setup composed of an inertial table and the following measurement and data acquisition instruments, as illustrated in “Figure 7”. An amplifier is connected at the input to a signal generator and at the output to a Modal Shop model 2025E Shaker. A 50 N load cell, HBM® model U9C, was installed at the end of the Shaker rod, and a displacement inductive sensor (LVDT (1)), HBM® model WI/20mm-T, was installed at the end of the rod. The load cell was firmly attached to a rigid rod, which was connected to the absorber device, with bearings at both ends to reduce undesired friction. To quantify the normal force on the absorber, an inductive displacement sensor (LVDT (2)), HBM®

model WI/10mm-T, was installed, which measured the deflection displacement of the spring with each tightening of the nut. The normal force was calculated by multiplying the compression spring stiffness constant by the deflection.

In the experimental procedure, a sinusoidal signal with a peak-to-peak amplitude of 200 mV was generated, and the frequency was varied between 2, 2.5, 3, 3.5, 4, and 4.5 Hz. Data acquisition was initiated only after the system reached steady-state conditions, which were collected using the Quantum-X system, and data analysis was performed using Matlab®. Additional tests were conducted using the same setup, but with varying amplitudes of 200 mV and 300 mV, at frequencies of 2 and 3 Hz.

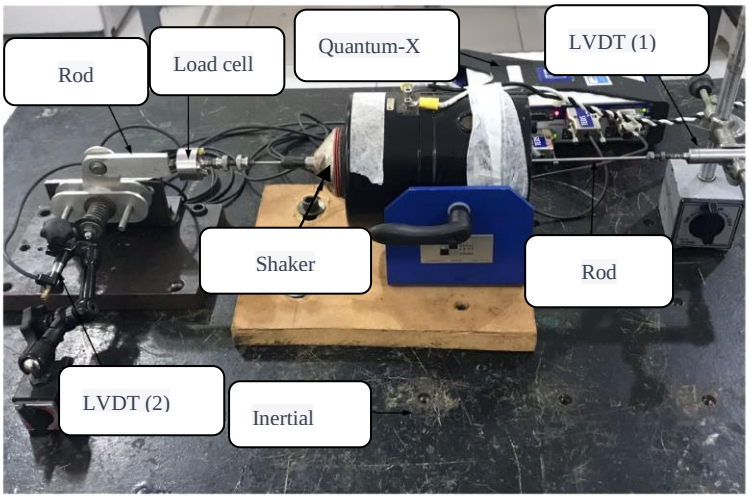

Figure 7 - Experimental setup with the damper device under forced vibration.

3.4. **Forced vibration measurement setup**

For the dynamic tests under forced vibration, the behavior of the structure was studied first with ADV locked, without any rotation friction. The experimental setup is depicted in “Figure 8”. After, the sequence of dynamic tests follows with the ADV unlocked. The input signal is a harmonic excitation with constant amplitude in 0.7mm. All tests followed the same measurement setup, performing excitation frequency in a sweep with range from 1.0 to 12Hz and increment of 0.05Hz. For each sweep cycles, the compression in the coil spring is increased by increment of 1mm in the spring deformation for each repletion of measurement.

For this forced vibration test, the structure was equipped with a PCB Piezotronics model 352B10 accelerometer, with a sensitivity of 10 mV/g. The accelerometer was installed in the position indicated in the photograph of "Figure 8". For the input excitation, an electromechanical vibration table of the Quanser® Shake Table II model, with 1 degree of freedom (1-DOF), was used. The input (table excitation) and output (acceleration response) signals were collected by the Keysight Technologies model 35670A dynamic signal analyzer, as shown in "Figure 8".

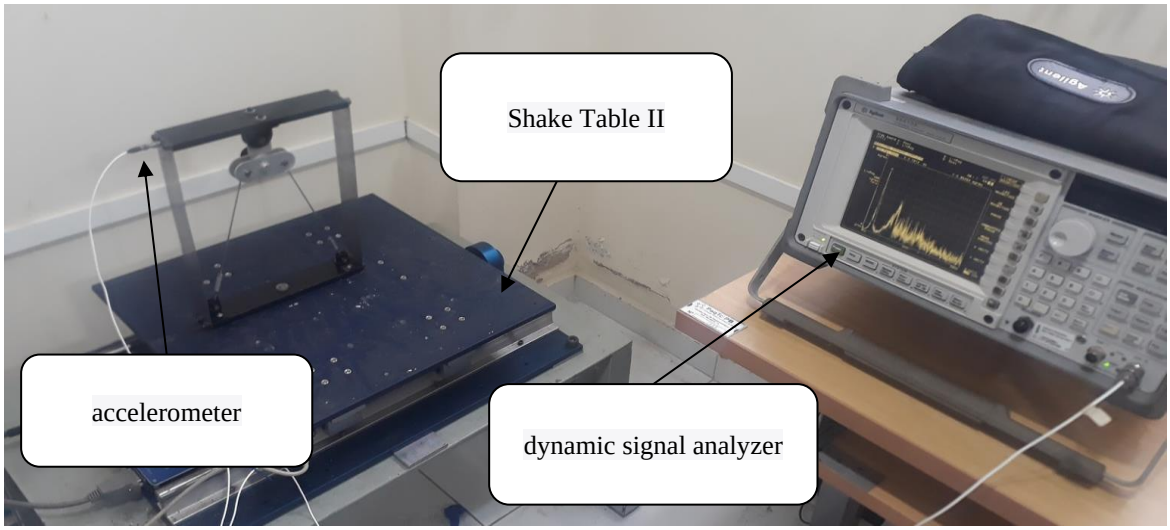

Figure 8 - Experimental setup of the system under forced vibration.

3.5. **Characterization of the structure with and without the use of the damper**

In the structure characterization test, illustrated in "Figure 9", it was equipped with a PCB Piezotronics model 352B10 accelerometer with a sensitivity of 10 mV/g. For the input excitation, the structure was laterally displaced by 15 mm. The output signals (acceleration response) were collected using the Quantum-X system, and data analysis was performed using Matlab®. In the setup with the energy dissipation device, the test was conducted without applying the compression spring displacement.

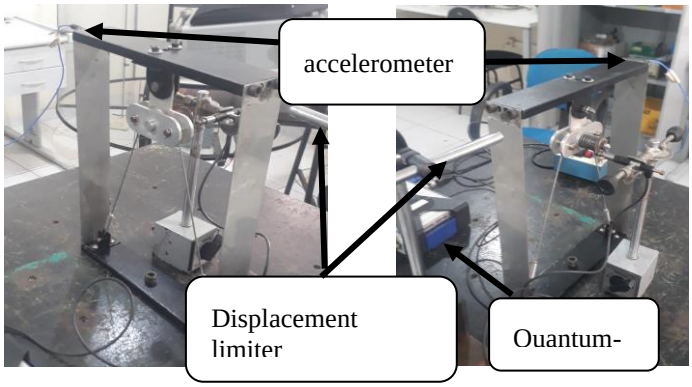

Figure 9 - Experimental setup for time response measurement.

4. **RESULTS**

4.1. **1 GDL frame characterization**

The results of tests on free vibration of the frame, in terms of response in frequency is presented in “Figure 10”, including both the responses from the experimental analysis as numeric.

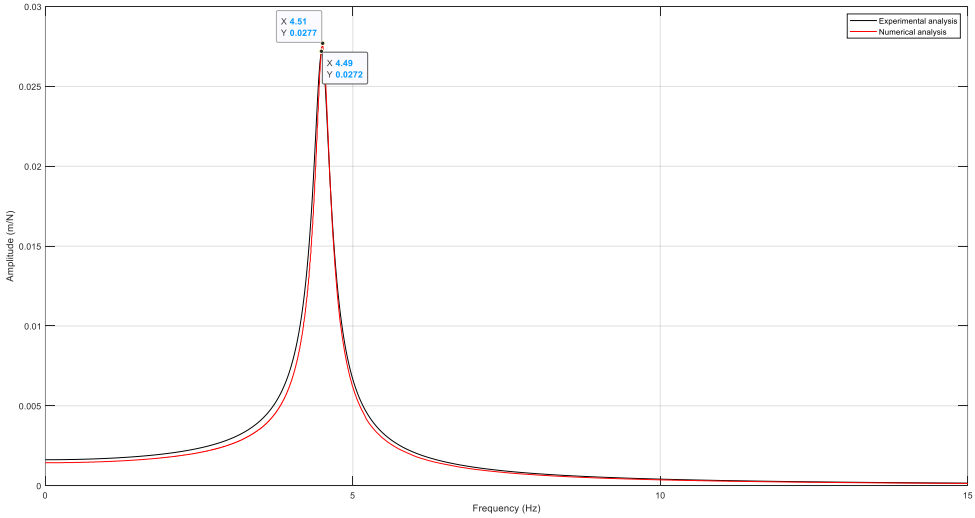

Figure 10 - Free vibration response of the frame without the damper.

Analyzing the results, it is observed that the curves practically coincide, especially in identifying the natural frequency of the system, presenting a small deviation, of the order of 0.2% between the curves, in relation to the trial value.

4.2. **Compression helical spring characterization**

Initially, the stiffness coefficient of the compression spring was calculated by the law of Hooke, whose test graph is represented in “Figure 11”. The stiffness result found experimentally it was 10448.26 N/m.

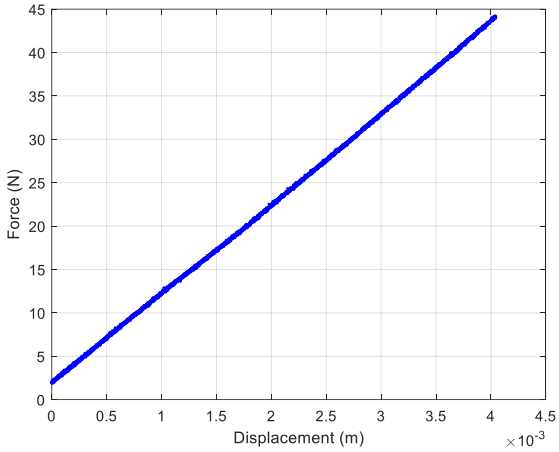

Figure 11- Graph of the compression spring stiffness curve.

4.3. **Characterization of the rotational friction damper**

"Figure 12" illustrates the forced vibration tests of the damper device to quantify the dissipated energy. The hysteretic damping is observed in the graph force versus displacement. The internal area of each graph corresponds to the dissipated energy. The same maximum force and amplitude are observed for each frequency tested.

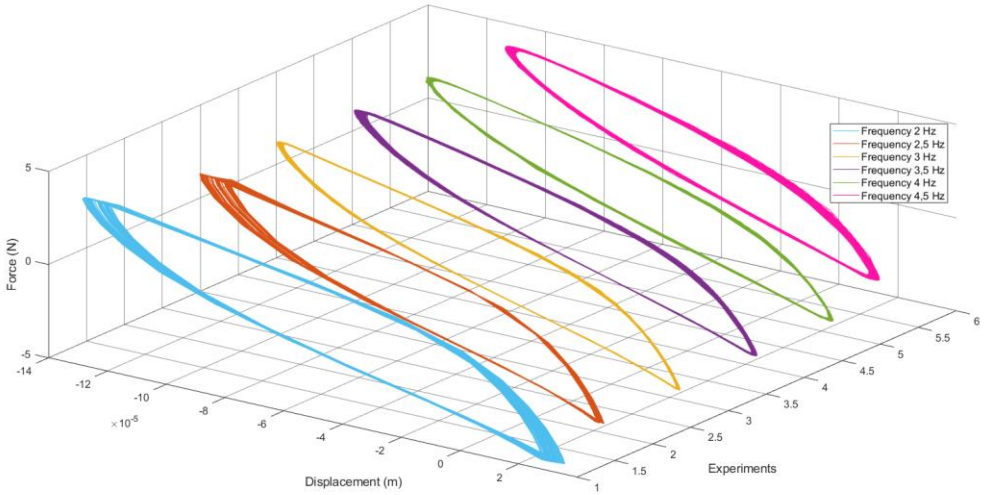

Figure12 - Energy dissipation graphs of the damper varying with frequency.

A comparison of the response with the variation of frequency at the same amplitude can be observed in "Table 1". It is possible to observe that the energy dissipation is of the same order of magnitude and practically constant for frequencies between 2.5 and 4 Hz.

Table 1-Data of energy dissipation varying with frequency.

Experiments	Frequency (Hz)	Average dissipated energy (J)
1	2.0	4.4685×10^{-4}
2	2.5	3.3404×10^{-4}
3	3.0	3.3349×10^{-4}
4	3.5	3.1907×10^{-4}
5	4.0	3.1535×10^{-4}
6	4.5	2.8765×10^{-4}

In “Figure 13”, where amplitudes and frequencies vary, from 2 to 3 Hz, an increase in the dissipated energy can be observed according to the amplitude variation.

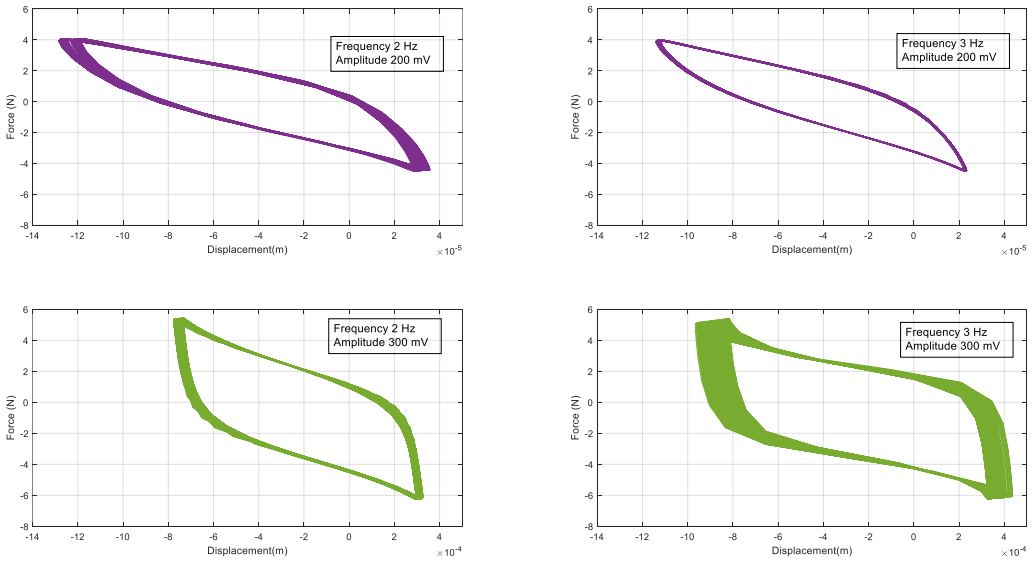

Figure 13 - Energy dissipation graphs of the damper varying with frequency and amplitude.

The comparative results of the quantification of energy dissipation are detailed in “Table 2”. As expected, there is an increase in energy dissipation with the increase in displacement amplitude.

Table 2 - Data of energy dissipation of the damper varying with frequency and amplitude.

Frequency (Hz)	Amplitude (mV)	Average dissipated energy (J)
2	200	4.4685×10^{-4}
3	200	3.3349×10^{-4}
2	300	7.0000×10^{-3}
3	300	5.4000×10^{-3}

4.4. **Forced vibration response**

The tests of the system under forced base vibration followed the criteria established previously in the experimental methodology, obtaining the Frequency Response Functions (FRFs) in the adopted configurations. The graphs in "Figure 14" illustrate the FRFs obtained for the system with and without the damper in different linear displacement configurations of the compression spring.

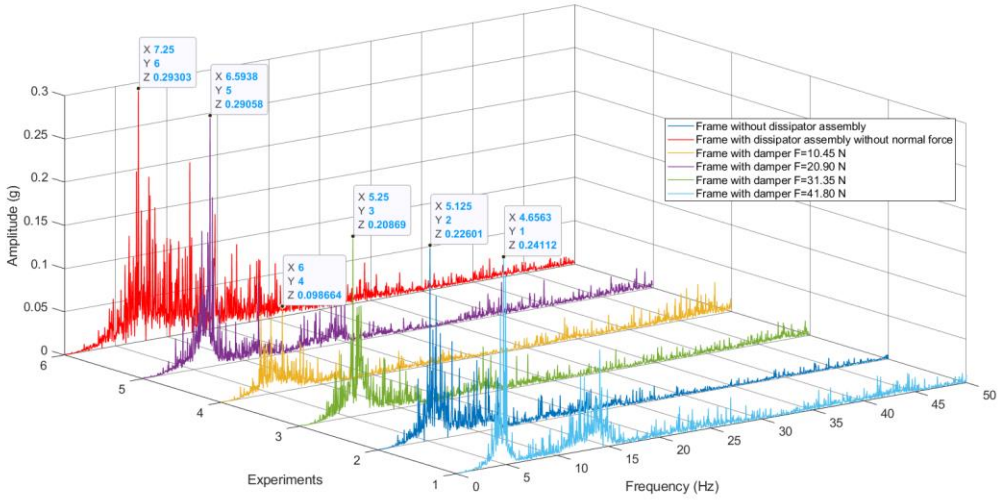

Figure 14- Frequency Response Functions.

As expected, the FRFs of the system with the incorporation of the rotational damper showed a significant reduction in displacement amplitude peaks, specially until 6 Hz, highlighting the high levels of mechanical energy dissipation in the system. It can be observed in "Table 3" up to which point the device is able to dissipate energy.

Table 3 - Dissipate energy x frequency.

Experiments	Condition	Frequency (Hz)	Amplitude (g)
1	Frame without the dissipator assembly.	4.656	0.24110
2	Frame with heatsink assembly without normal force.	5.125	0.22600
3	Frame with damper F=10.45 N.	5.250	0.20870
4	Frame with damper F=20.90 N.	6.000	0.09866
5	Frame with damper F=31.35 N.	6.594	0.29060
6	Frame with damper F=41.80 N.	7.250	0.29300

4.5. **Response to lateral displacement**

When analyzing the efficiency of the two configurations, one without the damper “Figure 15-a)” and the other with the incorporation of the rotational damper as a vibration absorber “Figure 15-b)”, it can be observed through the graphs presented in "Figure 15-b)" that the system with damper returns by static equilibrium in very few seconds.

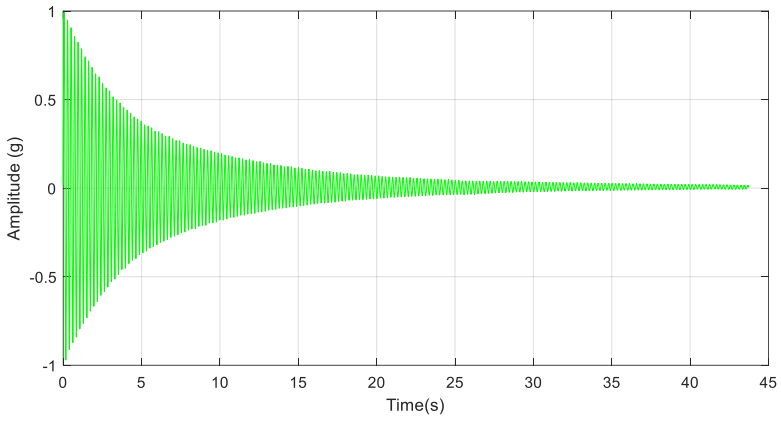

(a)

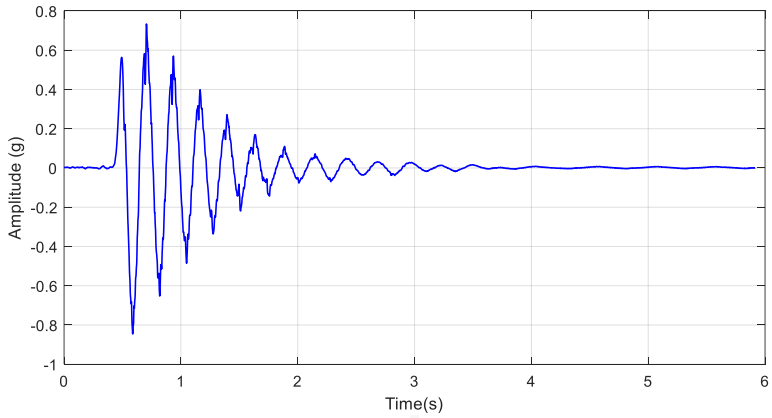

(b)

Figure 15 - Time response of the structure: (a) without the damper; (b) with the damper.

Through this response without the damper, one can observe an exponential decay typical of viscous damping, as shown in "Figure 15-a)", which lasts for more than 25 seconds, indicating that the frame structure has a damping factor of approximately 0,03. In "Figure 15-b)," the time response of the structure with the dissipative assembly installed

without the application of normal force is shown. The damping is characterized by the combination of frictional and viscous damping, with major damping factor, and it takes approximately 3 seconds to reach rest.

A comparison of the experimental response of the structure without the dissipative system and with the system installed, without the application of normal force, is illustrated in "Figure 16."

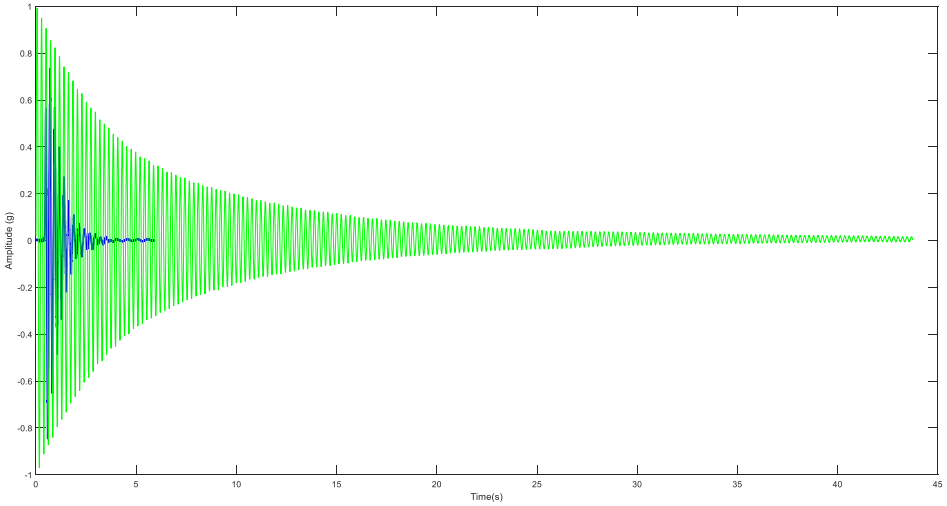

Figure 16 - The comparative experimental time responses.

5. CONCLUSION

It is concluded that there was success in characterizing the 1-DOF frame structure under forced vibration. It has been evaluated that the damper is effective when the normal force is up to 31.35 N, beyond which the device only adds stiffness to the structure. The results obtained for the characterization of the friction rotational damper indicate a similar and nearly constant average energy dissipation within the frequency range of 2.5 to 4 Hz. It is possible to observe that the energy dissipated by the damper is dependent on the variation in amplitude, with higher amplitudes resulting in greater energy dissipation.

6. ACKNOWLEDGEMENTS

The authors express their gratitude to the research funding agency CNPq, whose contribution was essential for the completion of this work. We would also like to thank the LVI - Laboratory of Vibrations and Instrumentation, which were used in the construction of the prototype and the LAMMEA - Multidisciplinary Laboratory of Materials and Active Structures – UAEM/UFCG, for providing the equipment used in the development of the prototype.

7. REFERENCES

Inman, D. J., 2013. Engineering Vibrations. Pearson, 4th edition.

Kim, J., Choi, H. and Min, K. W., 2011, Use of rotational friction dampers to enhance seismic and progressive collapse resisting capacity of structures. Struct. Design Tall Spec. Build, Vol. 20, pp. 515–537.

Moraes, Y. J. O., 2017. Dynamic analysis applied to passive vibration control in a portico-type structure incorporating super elastic nitinol mini-springs *(in Portuguese).* Master's thesis, Graduate Program in Mechanical Engineering, Federal University of Campina Grande, Campina Grande, Brazil.

Mualla, I. H., 2000, Experimental evaluation of new friction damper device. In 12th world conference on earthquake engineering, Auckland, New Zealand.

Norton, R.L., 1997. Machine Design - An Integrated Approach. Prentice Hall, New Jersey, 1st edition.

Rao, S., 2010. Mechanical vibrations. Prentice Hall, 5th edition.

8. RESPONSIBILITY NOTICE

Authors are solely responsible for the information included in this work